Bioactive Materials 15 (2022) 372–381

Contents lists available at ScienceDirect

Bioactive Materials

journal homepage: www.keaipublishing.com/en/journals/bioactive-materials

Magnetically responsive nanofibrous ceramic scaffolds for on-demand motion and drug delivery

Yonggang Zhang [a], Jiaping Li [a,b], Pamela Habibovic [a,*]

[a] Department of Instructive Biomaterials Engineering, Maastricht University, MERLN Institute for Technology-Inspired Regenerative Medicine, Universiteitssingel 40, 6229 ER, Maastricht, the Netherlands

[b] Department of Complex Tissue Regeneration, Maastricht University, MERLN Institute for Technology-Inspired Regenerative Medicine, Universiteitssingel 40, 6229 ER, Maastricht, the Netherlands

ARTICLE INFO

Keywords:
Hydroxyapatite
Magnetic
Responsive
Drug delivery
Cell culture

ABSTRACT

Smart biomaterials, featuring not only bioactivity, but also dynamic responsiveness to external stimuli, are desired for biomedical applications, such as regenerative medicine, and hold great potential to expand the boundaries of the modern clinical practice. Herein, a magnetically responsive three-dimensional scaffold with sandwich structure is developed by using hydroxyapatite (HA) nanowires and ferrosoferric oxide (Fe_3O_4) nanoparticles as building blocks. The magnetic HA/Fe_3O_4 scaffold is fully inorganic in nature, but shows polymeric hydrogel-like characteristics including a 3D fibrous network that is highly porous (>99.7% free volume), deformable (50% deformation) and elastic, and tunable stiffness. The magnetic HA/Fe_3O_4 scaffold has been shown to execute multimodal motion upon exposure to an external magnetic field including shape transformation, rolling and somersault. In addition, we have demonstrated that the magnetic scaffold can serve as a smart carrier for remotely controlled, on-demand delivery of compounds including an organic dye and a protein. Finally, the magnetic scaffold has exhibited good biocompatibility, supporting the attachment and proliferation of human mesenchymal stromal cells, thereby showing great potential as smart biomaterials for a variety of biomedical applications.

1. Introduction

Biomaterials have played an indispensable role in improving human life quality and extending life expectancy since ancient times. Historically, the role of biomaterials and the requirements they need to meet has undergone a continuous change. Untreated, nature-derived objects were the earliest biomaterials used in humans. For example, ancient Egyptians used natural cotton fibers and horsehair to suture wounds [1]. With the development of natural sciences and technology, untreated natural materials were gradually replaced by synthetic bioinert biomaterials. Examples of these are polymethylmethacrylate, polyethylene, polyesters and stainless steel, used in the middle of the 20th century as tooth, blood vessel and bone replacements [2]. By the end of the 20th century, a variety of bioactive materials that feature adaptiveness to the biological environment, has been developed. Bioactive biomaterials, designed to stimulate and/or direct appropriate cellular and tissue responses, have significantly promoted the development of modern medicine, including pharmacology, diagnosis, and regenerative medicine, among others [3]. In the past twenty years, the advances in micro- and nanotechnology and fabrication, along with an ever-growing interest in precision medicine, have triggered the emergence of next-generation "smart" biomaterials [4,5], which are not only bioactive, but also dynamically responsive to a variety of external stimuli, such as pH [6,7], acoustic signal [8,9], light [10–13], temperature [14,15], stress [16,17] and magnetism [18,19]. In particular, the use of magnetic fields has been suggested to be a safe and effective tool in biomedical applications for bioimaging and tissue engineering, since they can deeply penetrate the human body without attenuation [20,21]. To date, a variety of magnetically responsive three dimensional (3D) materials have been developed for various biomedical applications including on-demand drug delivery [22], mechanical stimulation of cells [23], as shape-memory [24] and shape-programmable scaffolds [25], and for targeted cargo transportation [20,26]. Despite these advancement that clearly show the potential of magnetically responsive

Peer review under responsibility of KeAi Communications Co., Ltd.
* Corresponding author.
E-mail address: p.habibovic@maastrichtuniversity.nl (P. Habibovic).

https://doi.org/10.1016/j.bioactmat.2022.02.028
Received 18 December 2021; Received in revised form 4 February 2022; Accepted 25 February 2022
Available online 5 March 2022

materials in minimally- or non-invasive surgery, as well as precision medicine, these studies have also shown room for further improvement. For example, Gong et al. successfully fabricated electrospun biodegradable composite nanofibers with magnetically actuated shape-memory effect by using poly(ε-caprolactone), carbon nanotubes and Fe_3O_4 nanoparticles, however, the extent of shape transformation was relatively limited [24]. Zhao et al. and Gilroy et al. developed alginate/Fe_3O_4 porous scaffold/hydrogel which could execute reversible deformations in response to magnetic stimulation. However, with an aim of obtaining desirable shape-transforming ability, large amount of Fe_3O_4 nanoparticles were used in both studies, resulting in a high Fe_3O_4/alginate mass ratio of 13:1 and 7:1, respectively, which impaired the biocompatibility of the scaffold/hydrogel [22,23]. Indeed, nearly 30% of dead cells were observed after 7 days of static culture on the hydrogels with the Fe_3O_4/alginate mass ratio of 7:1 [23]. Kim et al., Hu et al. and Lum et al. reported soft matter/robots with outstanding shape-transforming abilities by using silicone rubber and neodymium–iron–boron (NdFeB) particles as building blocks [20,25,26]. Nevertheless, the bioinert nature of these materials makes them unfavorable for biomedical applications, especially in vivo.

In the past few years, a family of advanced inorganic nanofibrous aerogels and inorganic nanofibrous sponges with exciting, untraditional properties including ultrahigh porosity (>99%), highly interconnected porous architecture with open cell geometry, large surface area, and elasticity have drawn significant attention as promising candidates for applications in many fields including tissue engineering, catalysis, protein separation and air purification [27–29]. Examples include SiO_2 nanofibrous aerogels [28], yttrium-stabilized ZrO_2 nanofibrous sponges [27], $BaTiO_3$ sponges [29], and hydroxyapatite (HA)/beta-tricalcium phosphate (β-TCP) nanofibrous sponges [30]. HA, more accurately, poorly crystalline substituted apatite is the main inorganic component of bone. Naturally derived and synthetic HA has been extensively investigated in the fields of bone defect repair and drug delivery, owing to its excellent biocompatibility and bioactivity [31–34]. Iron oxide nanoparticles, such as magnetite (Fe_3O_4), maghemite (γ-Fe_2O_3) and mixed ferrites have received attention due to their unique properties of being biodegradable and biocompatible, and have been employed for diagnostic and therapeutic purposes including magnetic resonance imaging, targeted delivery of drugs, biosensing and tissue regeneration [35].

In this work, we have developed a biocompatible, bioactive, magnetically responsive inorganic nanofibrous scaffold with sandwich structure which consists of a self-supporting network of seamlessly interwoven HA nanowires and a relatively small amount of ferrosoferric oxide (Fe_3O_4) nanoparticles. Previous studies reported inorganic magnetic scaffolds, such as akermanite-Fe_3O_4–CaO_2 scaffolds [36], magnetic mesoporous bioactive glass scaffolds [37], magnetic hardystonite scaffold [38], and magnetic calcium-zirconia scaffold [39]. In contrast to these materials, which were brittle and fragile, the magnetic scaffold developed here showed outstanding elasticity, despite being fully inorganic. In addition, despite -its inorganic nature, the magnetic scaffold showed great similarity to polymeric hydrogel materials including 3D nanofibrous network, high porosity, elasticity, and tunable stiffness. The magnetic HA/Fe_3O_4 scaffold was fabricated with a controllable amount and spatial distribution of Fe_3O_4 particles. The existence of relatively small amount of Fe_3O_4 particles endowed the scaffold with excellent magnetically responsive properties, without compromising its biocompatibility. For example, the scaffold displayed on-demand motion such as shape transformation, rolling and somersault upon exposure to an external magnetic field, which could not be achieved with previously reported magnetic hydrogels and magnetic polymeric scaffolds, such as magnetic poly(ethylene glycol) hydrogel [40], magnetic silk fibroin hydrogel/scaffold [41,42], magnetic polyglycolic acid scaffold [43], and magnetic poly(lactic acid) scaffold [44]. Although a few hydrogels and polymeric scaffolds with similar magnetically responsive property were reported, these studies have also shown room for further improvement of their biocompatibility [20,22,23,26]. The magnetic field induced deformation and volume variation allowed the magnetic HA/Fe_3O_4 scaffolds to be used as a carrier for various compounds including organic dye and protein, the release of which can be controlled on demand. The scaffold exhibited excellent biocompatibility supporting the attachment and proliferation of human mesenchymal stromal cells (hMSCs). Previous studies have illustrated positive effects of magnetically responsive scaffolds/gels on the preosteoblast proliferation [45], osteoblastic and vasculogenic potentials of tissue-engineered bone grafts [40], and osteogenic differentiation of mesenchymal stromal cells [46]. Therefore, we anticipate that the inorganic magnetic HA/Fe_3O_4 scaffold developed here with ultrahigh porosity, interconnected hierarchical pores with open cell geometry, extracellular matrix like nanofibrous 3D network, on-demand drug release property, as well as on-demand motion, might serve as a promising multifunctional platform for targeted drug delivery and bone regeneration.

2. Experimental section

Materials: Anhydrous calcium chloride (96%, Thermos Fisher), sodium oleate (≥82% (fatty acids), Sigma-Aldrich), ammonium phosphate dibasic (≥99%, Sigma Aldrich), iron (II,III) oxide (50–100 nm particle size, Sigma Aldrich), hemoglobin (Sigma Aldrich), methylene blue (VWR), sodium hydroxide (VWR).

Preparation of HA nanowire slurry: HA nanowire slurry was prepared by a hydrothermal method. Calcium chloride aqueous solution (0.16 M, 70 mL) was added into sodium oleate aqueous solution (0.58 M, 70 mL) and stirred for 1 h at room temperature, followed by the addition of ammonium phosphate dibasic aqueous solution (0.34 M, 56 mL). After 30 min, the resulting solution was evenly distributed over four 100 mL Teflon-lined stainless steel autoclaves. The autoclaves were sealed, heated in an oven to 200 °C and maintained at 200 °C for 24 h. Upon cooling of the autoclaves to room temperature, HA nanowire slurry was collected at the bottom of the Teflon autoclaves and kept in a plastic bottle for subsequent preparation of magnetic HA/Fe_3O_4 scaffolds. To determine the concentration of HA nanowires in the slurry, 5 mL of HA nanowire slurry was washed with ethanol and milliQ water, and dried. The concentration of HA nanowires in the slurry was calculated by dividing the volume of the HA nanowire slurry by the weight of HA nanowires in the slurry.

Preparation of regular magnetic HA/Fe_3O_4 scaffolds with different amount of Fe_3O_4: Desired amount of Fe_3O_4 nanoparticles was added into 10 mL of HA nanowire slurry with a concentration of 3 mg/mL, resulting in suspensions with the mass ratio of Fe_3O_4/HA being 2:1, 1:1 and 1:2, respectively. After treatment in ultrasonic bath for 1 h, the suspensions were frozen at - 20 °C in molds with desired shape and lyophilized. Then, the lyophilized samples were rinsed in ethanol (EtOH), water and treated in a NaOH–H_2O–EtOH solution (95 vol% ethanol and 5 vol% 10 M NaOH in water) at 90 °C for 72 h. The NaOH–H_2O–EtOH solution was refreshed every 24 h. Finally, the Fe_3O_4/HA scaffolds were washed with water and kept in water until further use.

Preparation of magnetic HA/Fe_3O_4 scaffolds with sandwich structure: First, desired amount of Fe_3O_4/HA slurry with the mass ratio of 2:1 was added into a cylindrical mold and kept at - 20 °C in a freezer for 30 min. Second, the mold was removed from the freezer and the same amount of Fe_3O_4/HA slurry with the mass ratio of 1:1 was added into the mold and immediately returned into the freezer. 30 min later, the same process as described for the second step was repeated with the Fe_3O_4/HA slurry with a ratio of 1:2. Finally, the samples were frozen at - 20 °C overnight and lyophilized and washed by using the above-mentioned method for regular HA/Fe_3O_4 scaffolds.

X-ray diffraction (XRD) analysis of HA, Fe_3O_4 and HA/Fe_3O_4 scaffolds: The XRD analysis of HA, Fe_3O_4 and HA/Fe_3O_4 scaffolds was performed using X-ray powder diffraction (Bruker D2 Phaser diffractometer, Cu Kα radiation, $\lambda = 1.5406$ Å) in the range of $10 \leq 2\Theta \leq 60°$ in increments of 0.02°and an integration time of 0.5 s.

Cyclic compression test: Cyclic compression test was performed on an

ElectroForce 3200 machine (ElectroForce 3200, USA), with a 45 N load cell. Cylindrical regular magnetic HA/Fe_3O_4 scaffolds and cylindrical magnetic HA/Fe_3O_4 scaffolds with sandwich structure with dimensions of Ø 11 × 11 mm were cyclically exposed to 50% compressive strain at a strain rate of 1 mm/s in water for 10 cycles. Three specimens were used for each sample type. The modulus of elasticity was defined as the slope of the linear region of the stress-strain curve after linear fit by using the Origin software.

Specific surface area and porosity analysis: The porosity of the regular magnetic HA/Fe_3O_4 scaffolds was calculated using the following equation:

$$\text{Porosity} = (1 - \rho_1/\rho_2) \text{ x } 100\% \quad (1)$$

$$\rho_1 = M_1/V_1 \quad (2)$$

$$\rho_2 = (\rho_{HA} \text{ x } \rho_{Fe3O4})/(W_2 \text{ x } \rho_{HA} + W_1 \text{ x } \rho_{Fe3O4}) \quad (3)$$

where M_1 and V_1 are the mass and volume of the regular magnetic HA/Fe_3O_4 scaffolds, respectively. ρ_{HA} represents the theoretical density of HA, which is 3.16 g cm^{-3}, and ρ_{Fe3O4} represents the theoretical density of Fe_3O_4, which is 5.18 g cm^{-3}. W_1 and W_2 are the mass fraction of HA and Fe_3O_4 in the regular magnetic HA/Fe_3O_4 scaffolds, respectively.

The specific surface area of the magnetic HA/Fe_3O_4 scaffolds with sandwich structure was characterized by a specific surface area analyzer (Micromeritics ASAP 2060, Germany).

On-demand dye release: A magnetic HA/Fe_3O_4 scaffold (Ø 11 × 5 mm) with sandwich structure was removed from water by using tweezers. A piece of tissue was gently placed on the surface of the scaffold to remove most of the water from the scaffold. The scaffold was allowed to absorb 100 μL of methylene blue aqueous solution with a concentration of 1 mg/mL by adding the solution dropwise on the top of the scaffold, and then placed into a cell culture dish with a diameter of 100 mm which was filled with 40 mL water, with the side having a Fe_3O_4/HA mass ratio of 1:2 facing the bottom. An electromagnet (1900 N, Conrad) was used to apply alternating magnetic field with a frequency of 0.25 Hz to the scaffold from the bottom. A scaffold to which no magnetic field was applied served as a control. Digital images of the culture dishes was captured at 0, 10, 20, 30, 60 min, respectively.

Protein adsorption and on-demand protein release: Magnetic HA/Fe_3O_4 scaffold (Ø 11 × 5 mm) with sandwich structure was removed from water by using tweezers. Water was removed from the scaffold by placing the scaffold onto a stack of paper tissue. Due to its high porosity and interconnected porous structure, the majority of water was removed from the scaffold within seconds. Next, the scaffold was placed in 3 mL of hemoglobin (Hb) aqueous solution with a concentration of 1.2 mg/mL at 37 °C for 24 h in a 15 mL centrifugation tube. Then, 1 mL of Hb solution was removed from the centrifugation tube and its UV–Vis absorption at a wavelength of 405 nm was measured (Agilent Cary 60 UV–Vis, the Netherlands). Subsequently, the scaffold was taken out of the centrifugation tube for on-demand protein release test. To remove the non-adsorbed Hb, the scaffold was first dried by paper tissues and then rinsed with milliQ water. This washing process was repeated twice. The scaffold was dried again by tissues and then placed in 3 mL of phosphate-buffered saline (PBS) solution with the side with Fe_3O_4/HA with a mass ratio of 1:2 facing the bottom. An electromagnet (1900 N, Conrad) was used to apply alternating magnetic field with a frequency of 0.25 Hz to the scaffold from the bottom side, while the scaffold that was not exposed to a magnetic field served as a control. At 1, 2, 3 and 4 h, respectively, 1 mL of the medium was collected and replaced by a fresh PBS solution. Finally, the collected release medium was analyzed for UV–Vis absorption at a wavelength of 405 nm.

Cell culture: hMSCs from one donor, obtained after written informed consent, were expanded in basic cell culture medium containing α-MEM (Gibco) with 10% FBS (Sigma), 0.2 mM ascorbic acid (Sigma), 100 U/mL penicillin and 100 mg/mL streptomycin (Gibco). Upon reaching confluency, the cells were frozen until further use. Cells at passage 6 were used for all the experiments.

Cylindrical magnetic HA/Fe_3O_4 scaffolds (Ø 6 × 6 mm) with sandwich structure saturated with water were dried using a piece of paper tissue and placed in wells of a 24-well plate. 100 μL of concentrated hMSCs suspension (Cell density: 200 x 10^4/mL) in basic cell culture medium was placed on top of the scaffolds. The medium was absorbed by the scaffold within several seconds. After 4 h incubation in a standard cell culture incubator, another 1.4 mL basic cell culture medium was added to each well, and complete refreshment of the medium was performed every 3 days.

Live/dead assay: For live/dead assay, after 24 h of culture, magnetic HA/Fe_3O_4 scaffolds with sandwich structure with cells were washed with PBS, and stained with Calcein-AM (Fisher Scientific) and ethidium homodimer-1 (EthD-1) (Fisher Scientific) in PBS for 30 min. The samples were washed with PBS and then observed using the fluorescence microscope (Nikon Eclipse Ti–S, Japan).

Quantification of metabolic activity: PrestoBlue kit (Thermo Fisher Scientific) was used to determine the metabolic activity of cells on scaffolds. Following culture for 7 or 14 days, the scaffolds (n = 4) were washed with 700 μL PBS. Then, PBS was removed and 700 μL PrestoBlue™ solution (10% in basic cell culture medium) was added to each well. After incubation in the dark at 37 °C for 30 min, 100 μL of incubated solution was transferred to a new black 96-well plate. The fluorescence was measured on the microplate reader (BMG Labtech CLARIOstar, Germany) at 590 nm.

Cell morphology: At day 7 and 14, scaffolds (n = 2) with cells were washed with PBS twice and fixed in 4% w/v formaldehyde (Sigma). After treatment with 0.1% v/v Triton X-100 (VWR), the scaffolds were washed with PBS three times, and then the nonspecific binding sites were blocked with 1 wt% bovine serum albumin (BSA, VWR). The cells were stained using Alexa Fluor 488 phalloidin (Fisher Scientific) and DAPI (Sigma-Aldrich). Finally, the morphology of cells on scaffolds was observed with a fluorescence microscopy (Nikon Eclipse Ti–S, Japan).

Statistical analysis: The data were presented as mean ± standard deviation and analyzed using GraphPad Prism 9 (GraphPad software, San Diego, USA). Unpaired Student's t-test was used to determine the statistical significance of the results. Significant differences were accepted when $p<0.05$ (indicated with (*) on the graphs).

3. Results and discussion

In this work, we have developed a magnetically-responsive fully inorganic nanofibrous scaffold, with mechanical and handling properties similar to those of polymeric (hydro)gels, by using HA nanowires and Fe_3O_4 nanoparticles as building blocks. The HA nanowires and Fe_3O_4 nanoparticles were phase-pure HA and magnetite, respectively (Fig. S1, Supporting Information). The fabrication process of the magnetic scaffolds (Fig. 1A) comprised the steps of the suspension formation between Fe_3O_4 nanoparticles and HA nanowire slurry, freezing, lyophilization, and removal of impurities. The as-prepared HA nanowire slurry comprised monodispersed HA nanowires because of the presence of oleate bilayer on the nanowire surface [47]. After adding Fe_3O_4 nanoparticles into the HA nanowire slurry and treatment in ultrasonic bath for 1 h, a uniform suspension consisting of Fe_3O_4 nanoparticles and HA nanowire was formed. During the freezing process, ice crystals formed in the suspension, inducing phase separation and self-assembly of the HA nanowires into a seamlessly interwoven highly porous network. Microscale Fe_3O_4 clusters, derived from Fe_3O_4 nanoparticles, were physically embedded in the nanofibrous network comprising HA nanowires (Figs. 1A and 2A). The amount of Fe_3O_4 nanoparticles in the magnetic HA/Fe_3O_4 scaffolds was highly tunable by changing the amount of Fe_3O_4 nanoparticles added to the HA nanowire slurry during the fabrication process, as illustrated in Fig. 1B and C. Here, we have fabricated magnetic HA/Fe_3O_4 scaffolds with the HA/Fe_3O_4 mass ratio of 1:2, 1:1 and 2:1, respectively. The amount of Fe_3O_4 nanoparticles did not have an obvious effect on the microstructure of the magnetic

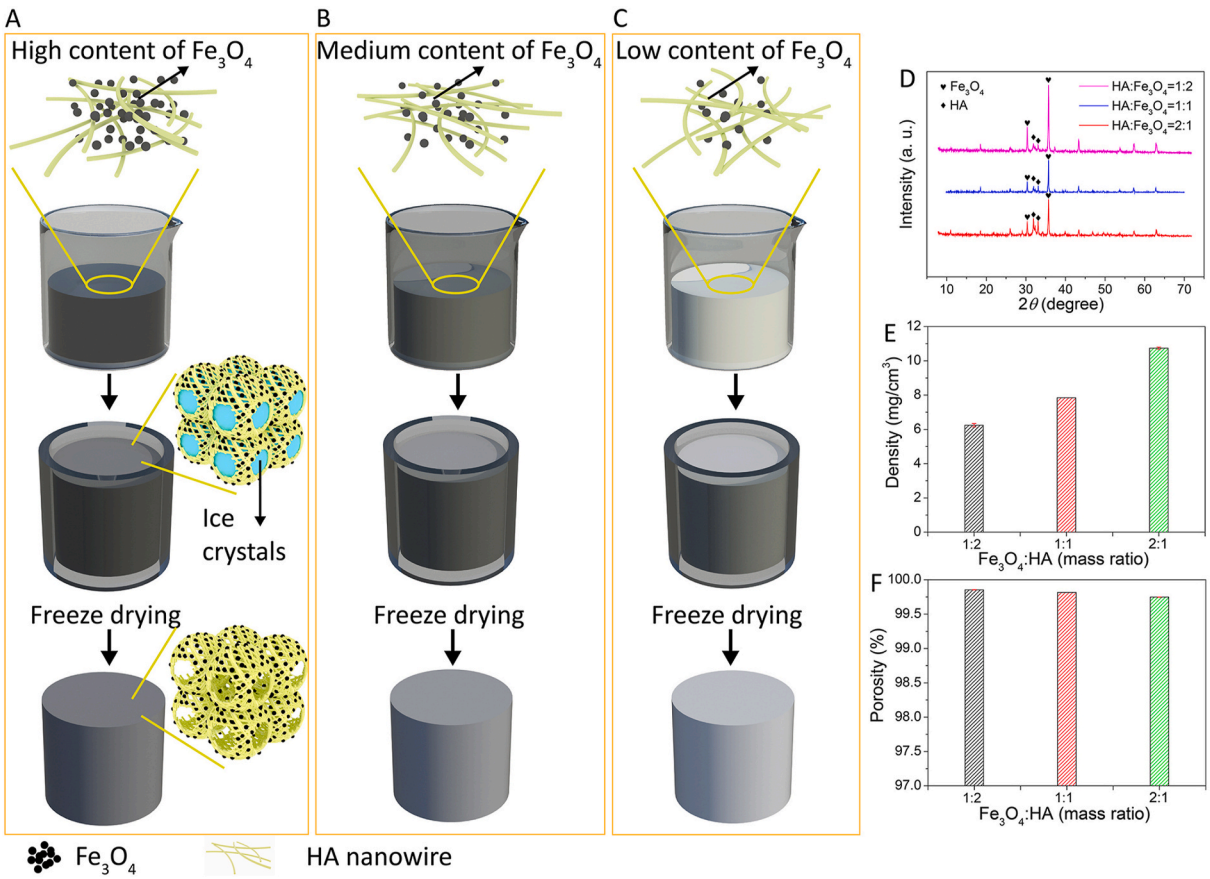

Fig. 1. (A,B,C) Schematic illustration of preparation process of magnetic HA/Fe_3O_4 scaffolds with different amounts of Fe_3O_4. (D,E,F) XRD patterns, density and porosity of magnetic HA/Fe_3O_4 scaffolds with the mass ratio of Fe_3O_4/HA of 2:1, 1:1 and 1:2, respectively.

HA/Fe_3O_4 scaffolds. All the magnetic HA/Fe_3O_4 scaffolds showed similar highly porous microstructure with open cell geometry and hierarchical pores ranging from hundreds of micrometers to several micrometers. The only obvious difference was a more abundant presence of Fe_3O_4 nanoparticles on the pore walls of scaffolds with a higher amount of Fe_3O_4 nanoparticles (Fig. 2, A, D and G).The intensity of the HA-specific diffraction peaks in the XRD patterns was higher in the scaffolds with lower amount of Fe_3O_4 particles (Fig. 1D). The scaffolds exhibited ultralow density and ultrahigh porosity ranging from 6.2 mg/cm^3 and 99.85%, respectively for 33.3% Fe_3O_4 to 10.7 mg/cm^3 and 99.75%, respectively for 66.7% Fe_3O_4 (Fig. 1E and F).

Despite the inorganic nature of HA nanowires and Fe_3O_4 nanoparticles, the as prepared magnetic HA/Fe_3O_4 scaffolds were not brittle, but instead exhibited an elastic behavior. The HA nanowires were shown to bend without collapsing/fracturing upon exposure to external loading, and to recover to their original shape when the loading was removed [30], suggesting that the unique elasticity of the magnetic HA/Fe_3O_4 scaffolds was derived from their flexible interwoven HA network. A 10-times repeated compression test on the same magnetic HA/Fe_3O_4 scaffolds in water was performed by applying 50% strain, to evaluate their structural stability and elasticity. As is shown by the stress-strain curves in Fig. 2, B, E and H, all the magnetic HA/Fe_3O_4 scaffolds, independent of their Fe_3O_4/HA mass ratio exhibited excellent resilience to compression and the ability to recover the porous structure after the release of pressure. The average elastic modulus of the magnetic HA/Fe_3O_4 scaffolds during the last five test cycles was calculated to be 3.46, 3.67, and 3.59 KPa for 66.7% Fe_3O_4, 50% Fe_3O_4, and 33.3% Fe_3O_4, respectively (Fig. 2, C, F, and I), indicating that the amount of Fe_3O_4 nanoparticles did not have an obvious effect on the stiffness of the scaffolds. A reason for this may be the fact that the Fe_3O_4 were dispersed within the HA nanowire network, thus providing a limited contribution to the mechanical properties of the HA/Fe_3O_4 scaffolds. In contrast, by increasing the concentration of HA nanowire slurry from 3 mg/mL to 5 mg/mL during the fabrication process, the stiffness of the magnetic HA/Fe_3O_4 scaffolds increased accordingly from 3.46 to 4.18 KPa, from 3.67 to 4.08 KPa, and from 3.59 to 4.16 KPa for 66.7%, 50%, and 33.3% Fe_3O_4, respectively (Fig. S2), because with a higher slurry concentration, a more dense HA network was formed. The elastic modulus of the HA/Fe_3O_4 scaffolds was lower than those of the HA nanowire aerogels and HA ceramic sponge reported earlier, because of the use of a relatively low concentration of HA nanowire slurry during the fabrication process [30,48]. Considering that the concentration of HA nanowire slurry was controllable during the synthetic process, it is plausible that the stiffness of the HA/Fe_3O_4 scaffolds developed here can further be tuned.

In addition to varying the amount of Fe_3O_4 nanoparticles among different samples, it was also possible to control the spatial distribution of Fe_3O_4 nanoparticles inside one scaffold. For example, we fabricated a magnetic HA/Fe_3O_4 scaffold with sandwich structure consisting of three different layers with the mass ratio of Fe_3O_4/HA being 2:1, 1:1 and 1:2, respectively. The fabrication process of the magnetic HA/Fe_3O_4 sandwich scaffold was similar to that of the regular scaffolds, with the exception that the middle step of suspension freezing inside a mold was divided into three substeps, with at each substep the addition of the suspension with different mass ratio of Fe_3O_4/HA (Fig. 3A). In detail, 300 μL of suspension of HA/Fe_3O_4 (mass ratio of 2:1) was added into the bottom of a cylindrical mold with a diameter of 10 mm to serve as the first layer and kept at - 20 °C in a freezer for 30 min. During the freezing process, the viscosity of the suspension increased as the temperature decreased while it still maintained in liquid state. Subsequently, 300 μL

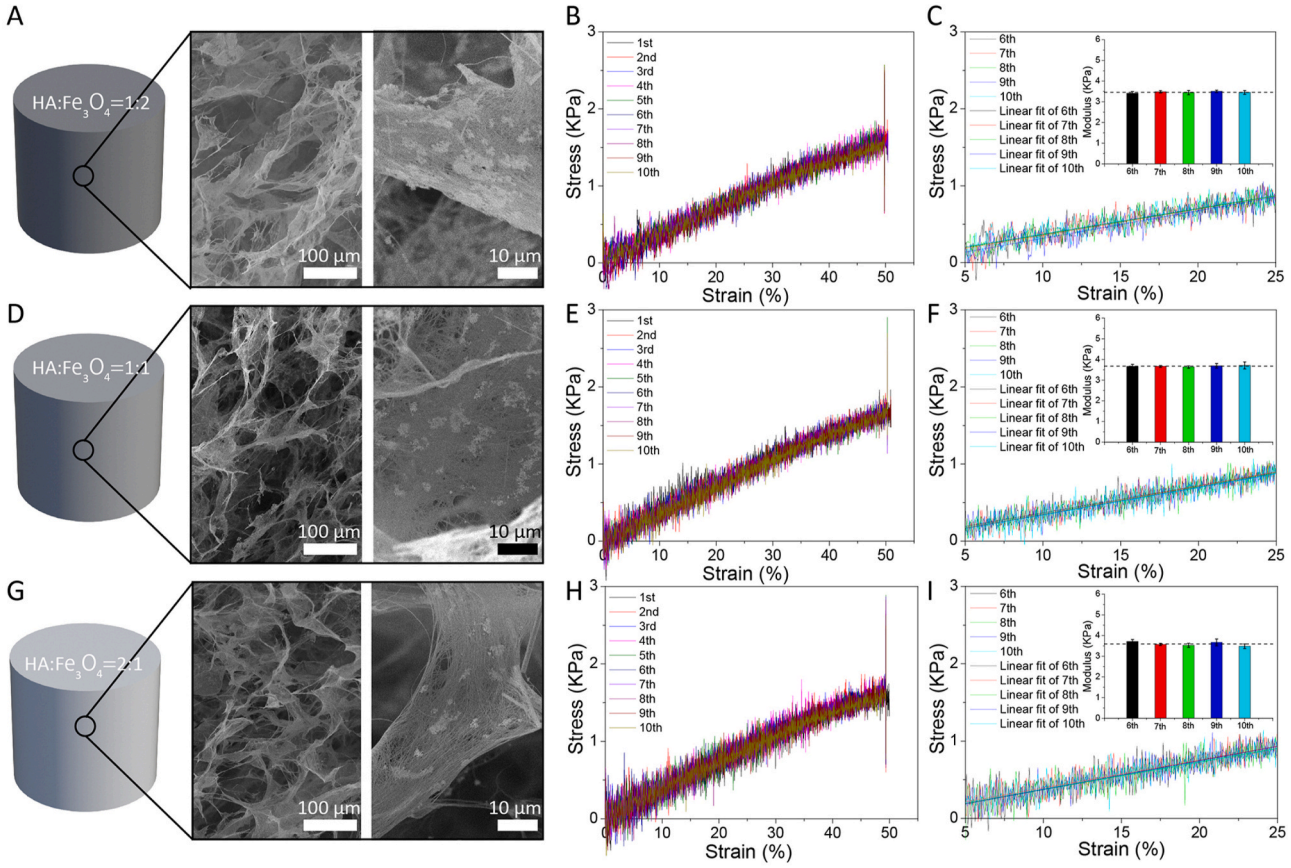

Fig. 2. (A,D,G) SEM micrographs and (B,E,H) the 10-times uniaxial compression stress–strain curves of the magnetic HA/Fe_3O_4 scaffolds with the Fe_3O_4/HA mass ratio of 2:1, 1:1 and 1:2, respectively. (C,F,I) Linear fit of the linear region of the stress-strain curves and compressive modulus of magnetic HA/Fe_3O_4 scaffolds with the Fe_3O_4/HA mass ratio of 2:1, 1:1 and 1:2, respectively, during the last five compression tests with 50% strain.

of suspension of HA/Fe_3O_4 (mass ratio of 1:1) was added into the mold. Since the freshly added suspension of HA/Fe_3O_4 (mass ratio of 1:1) had a lower density and lower viscosity compared to those of the first layer, a stable second layer was formed while preserving a good structural integrity of the first layer. The same process as described for the second layer was repeated to fabricate the last layer by using the Fe_3O_4/HA slurry with a ratio of 1:2. Finally, the samples were frozen at - 20 °C overnight and lyophilized. The magnetic HA/Fe_3O_4 sandwich scaffold was also highly elastic with interconnected porous structure with open cell geometry. These interconnected cellular pores could serve as a reversible water reservoir, allowing water to flow out of and into the scaffold by applying cyclic compression (Fig. 3B and C and D). The magnetic HA/Fe_3O_4 sandwich scaffold showed a similar trend of stress-strain curves during the 10-times repeated compression test. The average elastic modulus of the last five tests was 3.32 KPa, which is comparable to those of regular magnetic HA/Fe_3O_4 scaffolds (Fig. 3E and F and G).

Taken together, we have developed fully inorganic, soft and elastic magnetic scaffolds with tunable stiffness, and controlled amount and spatial distribution of magnetic nanoparticles using a simple freeze-drying method. The magnetic Fe_3O_4/HA scaffolds in water exhibited physical properties similar to those of polymeric hydrogel materials featuring 3D nanofibrous network, tunable stiffness, high porosity and good elasticity (Table S1, Supporting Information). In addition, the magnetic Fe_3O_4/HA scaffolds had a specific surface area of 24.39 m^2/g, which is in the range of what was previously reported for some hydrogels [49,50].

Fe_3O_4 nanoparticles are superparamagnetic, meaning that they are magnetic when exposed to an external magnetic field, but no longer magnetic when the magnetic field is removed. As a result, materials containing superparamagnetic Fe_3O_4 nanoparticles can be guided by an external magnetic field gradient or alternating magnetic field to perform a variety of on-demand activities, including movement, accumulation, hyperthermia and drug release [35]. In this work, the presence of Fe_3O_4 nanoparticles endowed the HA/Fe_3O_4 sandwich scaffolds with the ability to execute on-demand multimodal motion, including shape change, rolling and somersault upon exposure to an external magnetic field. As is shown in Fig. 4A, a cylindrical HA/Fe_3O_4 sandwich scaffold (Ø 6 × 6 mm) was placed in water with the side with the Fe_3O_4/HA mass ratio of 1:2, thus the side with the lowest amount of magnetic nanoparticles, facing the bottom. When a cylindrical magnet (Ø 40 × 20 mm) approached the bottom of the dish containing the scaffold, the scaffold transformed from relaxed state to a compressed state automatically, and recovered to its original shape when the magnet was removed (Supplementary Movie 1). For the magnetic stimulation, the magnet was placed underneath the magnetic scaffold, thus on one side of the scaffold. As a result, the magnetic attraction force on the magnetic particles and the resulting compression force on the scaffold were not balanced over the entire height of the scaffold. To compensate for this, a sandwich structure was used, with the layer containing the lowest amount Fe_3O_4 particles serving as the bottom layer, closest to the magnet. Besides this shape transformation, the HA/Fe_3O_4 sandwich scaffold was able to make more complex movements like somersault (Fig. 4B, Supplementary Movie 2) and rolling (Fig. 4C, Supplementary Movie 3) and move in the desired direction by placing a mobile magnet at a certain distance from the scaffold.

It is noteworthy that due to the tunable stiffness of the inorganic network and controllable spatial distribution of Fe_3O_4 nanoparticles in the scaffold, the total amount of Fe_3O_4 nanoparticles needed to achieve a good shape-transforming ability (Fe_3O_4: HA ratio 1:1) was considerably

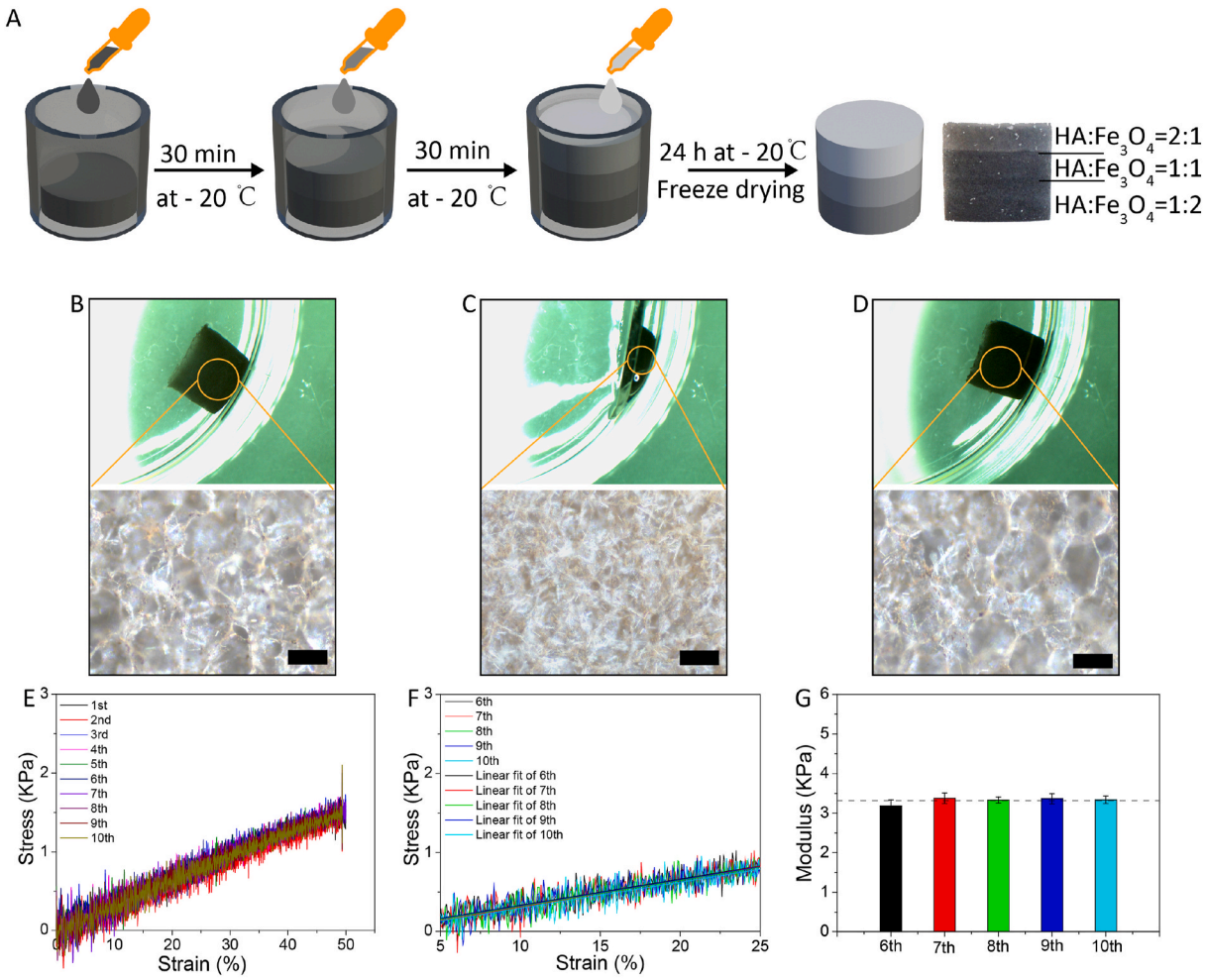

Fig. 3. (A) A schematic illustration of magnetic HA/Fe_3O_4 sandwich scaffold production. (B,C,D) Digital and microscopic images of a magnetic HA/Fe_3O_4 sandwich scaffold in the original shape, compressed shape and recovered shape. (E,F,G) The 10-times uniaxial compression stress–strain curves, linear fit of the linear region of the stress-strain curves and compressive modulus of magnetic HA/Fe_3O_4 sandwich scaffold during the last five compression tests with 50% strain. Scale bar: 100 μm.

lower than what was reported in previous studies (7:1 and 13:1) [22,23]. This is an advantage, since it has been shown that an excess of Fe_3O_4 nanoparticles might be toxic to cells [23]. Moreover, the interwoven network of HA/Fe_3O_4 sandwich scaffold consisted of bioactive HA crystals [51], rather than bioinert silicone rubber as was used in many studies [20,25,26].

Taken together, the remote actuation by magnetic fields of such an inorganic, highly porous and fast shape-shifting soft materials with good biocompatibility offers new possibilities for applications in biomedical devices, materials for regenerative medicine and soft robotics. As a proof of concept, in the next section, we demonstrated that the HA/Fe_3O_4 sandwich scaffolds can be used as a smart carrier for different cargos.

In the past decade, the development of bioactive, smart, and multi-functional drug carriers for integrated diagnosis and treatment approaches and targeted and on-demand drug delivery has been a topic of great interest, to address clinical challenges related to, e.g., cancer, diabetes and infections [52–55]. We hypothesized that the magnetic field-induced shape transformation and resulting water convection, associated with the shear stress, can promote dissociation of drugs from and enhance transport of unbound drugs out of the porous structure, thus accelerating the release of drugs loaded on the HA/Fe_3O_4 sandwich scaffolds (Fig. 5A). To test this hypothesis visually, we first used methylene blue dye-loaded HA/Fe_3O_4 sandwich scaffolds as a model. As is shown in Fig. 5B, without magnetic field stimulation, the methylene blue dye was released slowly from the scaffold in a typical physical diffusion manner, i.e., diffusion of the dye molecules from high concentration to low concentration occurred, forming a gradient of blue color around the scaffold. In contrast, a much faster release and more uniform distribution of the methylene blue dye was observed when an alternating magnetic field was applied to the HA/Fe_3O_4 sandwich scaffold (Fig. 5C). Under the magnetic field stimulation, the HA/Fe_3O_4 sandwich scaffold analogous to a beating heart, thereby 'pumping' the methylene blue dye out of its porous structure. In addition, the water convection caused by the shape transforming activity of the magnetic scaffold may have accelerated the diffusion rate of the methylene blue molecules. As a consequence, the HA/Fe_3O_4 sandwich scaffold showed a much faster release of the methylene blue dye upon stimulation by the magnetic field compared to that of the static one.

We then chose Hb as a model drug. The UV–vis absorption measurements at 405 nm of the Hb solution before and after immersion of an HA/Fe_3O_4 sandwich scaffold is shown in Fig. 5D. Due to the ultrahigh porosity and hierarchical porous architecture, the Hb loading capacity of HA/Fe_3O_4 sandwich scaffold was as high as 71.3 ± 3.6 μg/mg, which was much higher than that of HA porous ceramics and octacalcium phosphate/poly(lactic-co-glycolic acid) scaffold studied earlier [56,57]. The Hb loaded HA/Fe_3O_4 sandwich scaffolds were then placed in a PBS solution, and one group of the scaffolds was subjected to the magnetic field with a frequency of 0.25 Hz, while no magnetic field was applied to the other group. The cumulative release of Hb from the HA/Fe_3O_4 sandwich scaffolds exposed to magnetic stimulation for 4 h was 64.2 ± 3.9 μg (13.8% of total amount), which was about twice as high as that of HA/Fe_3O_4 sandwich scaffolds without magnetic stimulation (Fig. 5E).

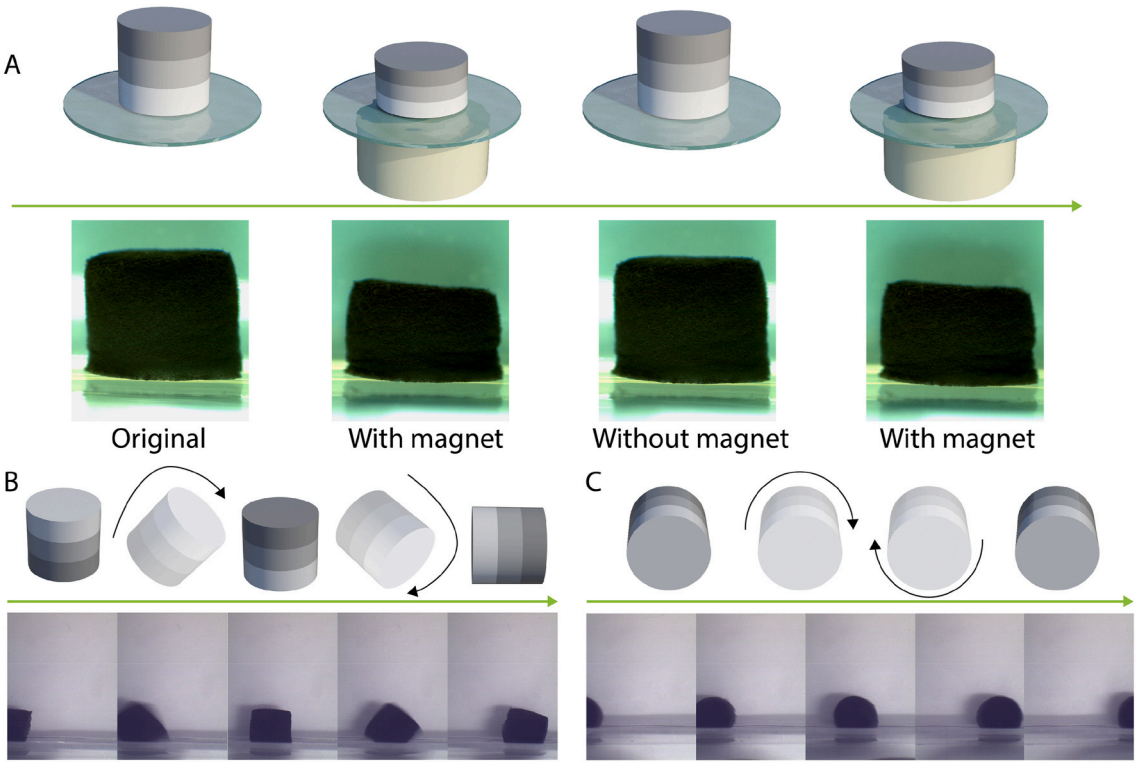

Fig. 4. (A) Schematic representation and images of the process of shape transformation of HA/Fe_3O_4 sandwich scaffolds induced by the intermittent presence of magnetic field. (B,C) Schematic representation and images of the HA/Fe_3O_4 sandwich scaffolds performing a somersault (B) and rolling (C) movement induced by a mobile magnet.

The average release rate of Hb from the two groups of samples at each time point during 4 h is shown in Fig. 5F, demonstrating that the release rate upon magnetic stimulation was higher than in the absence of magnetic stimulation throughout the experiment. We propose that the mechanism underlying the accelerated release of the methylene blue dye from the magnetically-stimulated scaffold is also valid for the release of Hb molecules from the HA/Fe_3O_4 sandwich scaffold, with the difference that the Hb molecules were preloaded on HA/Fe_3O_4 sandwich scaffold by adsorption, while methylene blue dye solution was loaded in the pores of HA/Fe_3O_4 sandwich scaffold by absorption.

Taken together, the HA/Fe_3O_4 sandwich scaffold with magnetically responsive shape transformation ability might serve as a promising smart drug carrier for magnetically controlled drug release.

Finally, the biocompatibility of the HA/Fe_3O_4 sandwich scaffolds was assessed by live/dead staining, measuring the metabolic activity and observing the morphology of hMSCs cultured on them. The live/dead assay was performed by staining the cells cultured for 24 h on the HA/Fe_3O_4 sandwich scaffold with Calcein-AM and ethidium homodimer-1 (EthD-1). As shown in Fig. S3 (Supporting Information), in different layers of the HA/Fe_3O_4 sandwich scaffolds, the cells showed intense green fluorescence and the number of dead cells was negligible. In the study by Gilroy et al., the rat MSCs cell death after 7-day static culture on a magnetically responsive shape-transforming hydrogel with an Fe_3O_4/alginate mass ratio of 7:1, was nearly 30% [23]. Zhao et al. developed an alginate/Fe_3O_4 porous scaffold with the mass ratio of Fe_3O_4/alginate being 13:1, which could execute reversible deformations in response to magnetic stimulation. In this study, nearly 5% of human dermal fibroblasts were dead after 4 h of co-culture [22]. In our study, the metabolic activity of hMSCs cultured on HA/Fe_3O_4 sandwich scaffolds for 14 days was significantly higher than that of the cells cultured for 7 days, suggesting that the cells were able to proliferate on the HA/Fe_3O_4 sandwich scaffolds (Fig. S4, Supporting Information). A similar trend of increase in cell number was observed by proliferation test of other magnetic scaffolds with much lower amount of Fe_3O_4 nanoparticles (<10 wt%) [58,59]. To further investigate the biocompatibility of the HA/Fe_3O_4 sandwich scaffolds, the attachment and morphology of hMSCs cultured for 7 and 14 days were studied using fluorescence staining and microscopy. At day 7, the cells were abundant and homogenously distributed on both sides and the periphery of the HA/Fe_3O_4 sandwich scaffolds, as illustrated by the low-magnification (4X) fluorescence image (Fig. S5, Supporting Information). As shown on the higher magnification (10X) fluorescence images (Fig. 6A–C), the cells exhibited a spread morphology, with long filopodia and actin cytoskeleton taking the shape of the underlying nanofibrous material. At day 14, a similar observation was made, with more cells present and a more elongated actin cytoskeleton morphology (Fig. S6 (Magnification 4X) and Fig. S7 (Magnification 10X), Supporting Information). Therefore, the HA/Fe_3O_4 sandwich scaffolds showed good biocompatibility.

It is noteworthy that the magnetic-field-induced shape transformation and resulting water convection could generate associated compression force and shear force. Considering the fact that the HA/Fe_3O_4 sandwich scaffolds showed good biocompatibility, supporting cell proliferation and attachment, we anticipate that the scaffolds developed here may also serve as a unique 3D model for the study of mechanical stimulation of cells in a non-invasive manner [23]. We intend to use our HA/Fe_3O_4 sandwich scaffolds as intrinsically-deformable bioreactors to study mechanical stimulation of cells for bone tissue engineering applications.

4. Conclusion

In this work, a magnetically-responsive inorganic nanofibrous scaffold was developed by using anisotropic HA nanowires and Fe_3O_4 nanoparticles as building blocks. The scaffold was soft and elastic, rather than brittle, and showed similarities to polymeric hydrogel materials in physical properties including porosity and tunable modulus despite its inorganic nature. The amount and distribution of the Fe_3O_4 nanoparticles in the porous structure could easily be varied, to create

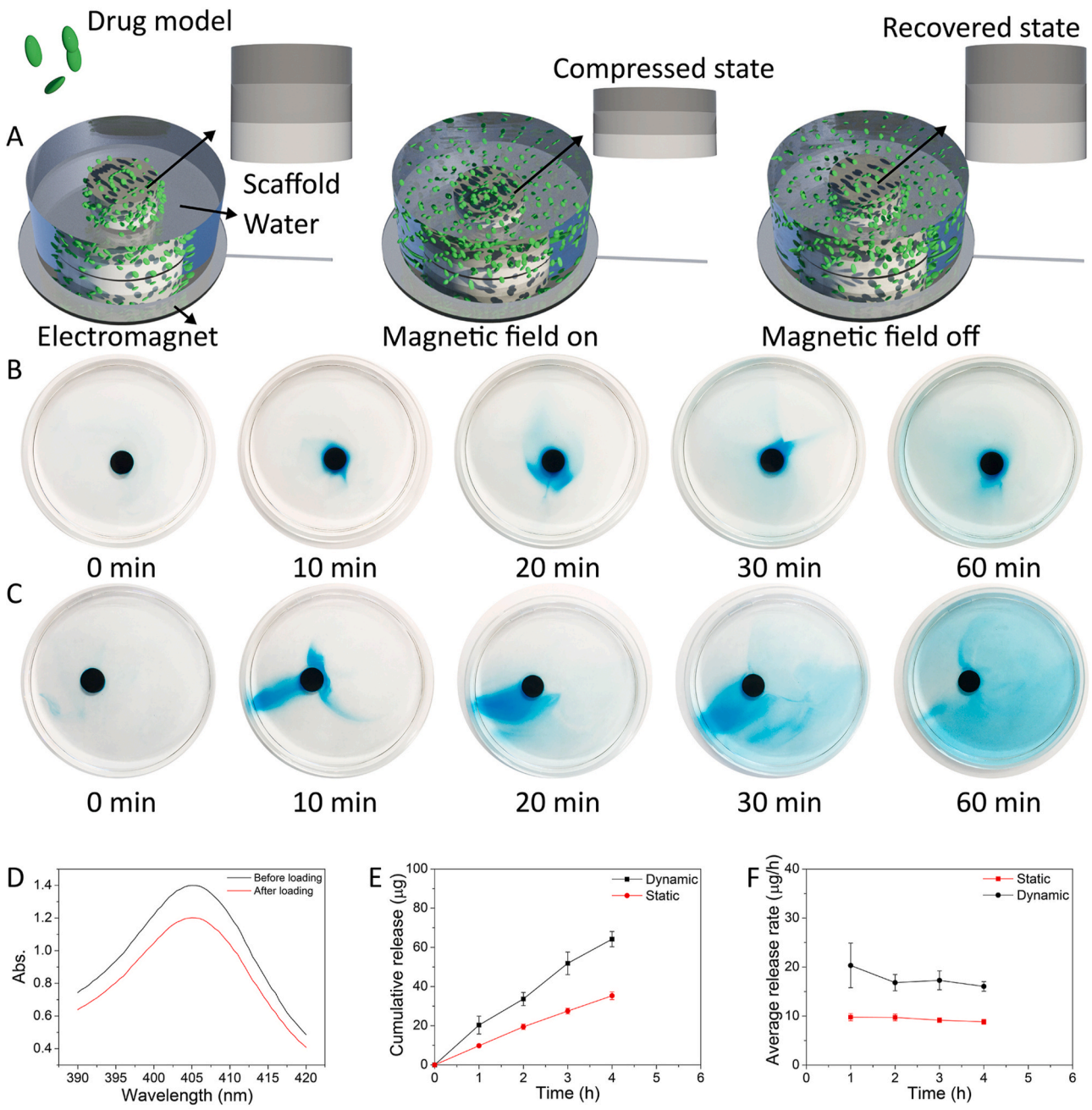

Fig. 5. (A) Schematic representation of the process of on-demand drug release of HA/Fe_3O_4 sandwich scaffolds induced by alternating magnetic field. (B,C) Images of methylene blue dye release from HA/Fe_3O_4 sandwich scaffolds without (B) and with (C) magnetic stimulation within 1 h. (D) UV–vis absorption spectra of the Hb solution before and after immersion of an HA/Fe_3O_4 sandwich scaffold. (E) Cumulative release profiles over 4 h of Hb from HA/Fe_3O_4 sandwich scaffolds subject to magnetic stimulation, or without magnetic stimulation. (F) Average Hb release rate of HA/Fe_3O_4 sandwich scaffolds subjected to magnetic stimulation, or without stimulation at different time points within 4 h.

scaffolds with a sandwich structure with layers containing different amounts of magnetic nanoparticles. A much lower amount of Fe_3O_4 nanoparticles compared to those used in other studies could efficiently endow the HA/Fe_3O_4 sandwich scaffolds with the ability to execute on-demand multimodal motion such as shape transformation (compression), rolling, somersault and displacement upon exposure to an external magnetic field. The compression and related volume variation made the HA/Fe_3O_4 sandwich scaffold suitable for carrying and releasing organic compounds upon remote control by a magnet. Finally, the use of HA crystals and small amount of Fe_3O_4 nanoparticles endowed the HA/Fe_3O_4 sandwich scaffolds with superior biocompatibility compared to that of other magnetically responsive materials made from bioinert building blocks. Taken together, the HA/Fe_3O_4 sandwich scaffolds developed here offers new possibilities for applications in biomedical devices, materials for regenerative medicine and soft robotics, especially in targeted drug delivery and bone regeneration.

CRediT authorship contribution statement

Yonggang Zhang: Conceptualization, Methodology, Validation, Formal analysis, Investigation, Data curation, Writing – original draft, Writing – review & editing, Visualization. **Jiaping Li:** Methodology, Validation, Investigation, Writing – review & editing. **Pamela Habibovic:** Methodology, Writing – review & editing, Visualization,

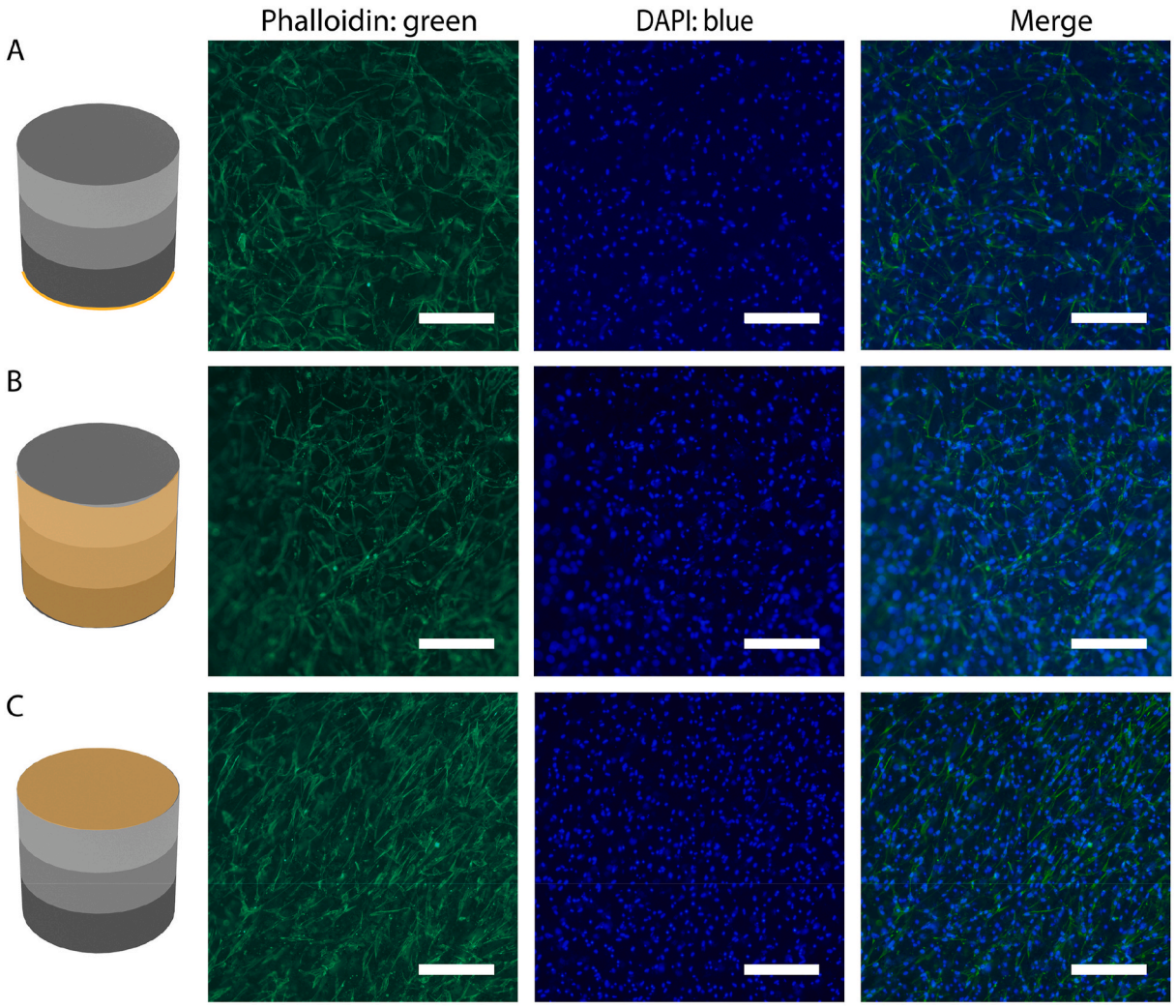

Fig. 6. Actin cytoskeleton (phalloidin: green) and nuclei (DAPI: blue) staining of hMSCs cultured on HA/Fe_3O_4 sandwich scaffolds for 7 days. Scale bar: 250 μm.

Supervision, Project administration, Funding acquisition.

Declaration of competing interest

The authors declare that they have no known competing interests.

Acknowledgements

This research was financially supported by the Gravitation Program "Materials Driven Regeneration", funded by the Netherlands Organization for Scientific Research (NWO) (Grant #024.003.013). JL and PH acknowledge financial support by the NWO, Applied and Engineering Sciences (NWO-AES, Grant #16711).

Appendix A. Supplementary data

Supplementary data to this article can be found online at https://doi.org/10.1016/j.bioactmat.2022.02.028.

References

[1] T.M. Muffly, A.P. Tizzano, M.D. Walters, J. R. Soc. Med. 104 (2011) 107.
[2] C.Y. Hu, T.-R. Yoon, Biomater. Res. 22 (2018) 33.
[3] V.J. Shirtliff, L.L. Hench, J. Mater. Sci. 38 (2003) 4697.
[4] A.B. Shodeinde, A.C. Murphy, H.F. Oldenkamp, A.S. Potdar, C.M. Ludolph, N. A. Peppas, Adv. Funct. Mater. 30 (2020), 1909556.
[5] Y. Lu, A.A. Aimetti, R. Langer, Z. Gu, Nat. Rev. Mater. 2 (2016) 16075.
[6] D. Schmaljohann, Adv. Drug Deliv. Rev. 58 (2006) 1655.
[7] W. Tao, J. Wang, W.J. Parak, O.C. Farokhzad, J. Shi, ACS Nano 13 (2019) 4876.
[8] A.G. Athanassiadis, Z. Ma, N. Moreno-Gomez, K. Melde, E. Choi, R. Goyal, P. Fischer, Chem. Rev. (2021), https://doi.org/10.1021/acs.chemrev.1c00622.
[9] S.R. Sirsi, M.A. Borden, Adv. Drug Deliv. Rev. 72 (2014) 3.
[10] X. Li, J.F. Lovell, J. Yoon, X. Chen, Nat. Rev. Clin. Oncol. 17 (2020) 657.
[11] Y. Liu, P. Bhattarai, Z. Dai, X. Chen, Chem. Soc. Rev. 48 (2019) 2053.
[12] Z. Li, X. Zhang, J. Ouyang, D. Chu, F. Han, L. Shi, R. Liu, Z. Guo, G.X. Gu, W. Tao, L. Jin, J. Li, Bioact. Mater. 6 (2021) 4053.
[13] J. Ouyang, X. Ji, X. Zhang, C. Feng, Z. Tang, N. Kong, A. Xie, J. Wang, X. Sui, L. Deng, Y. Liu, J.S. Kim, Y. Cao, W. Tao, Proc. Natl. Acad. Sci. U.S.A. 117 (2020) 28667.
[14] Z. Al-Ahmady, K. Kostarelos, Chem. Rev. 116 (2016) 3883.
[15] H.J. Moon, D.Y. Ko, M.H. Park, M.K. Joo, B. Jeong, Chem. Soc. Rev. 41 (2012) 4860.
[16] A. Marino, G.G. Genchi, V. Mattoli, G. Ciofani, Nano Today 14 (2017) 9.
[17] J. Jacob, N. More, K. Kalia, G. Kapusetti, Inflamm. Regen. 38 (2018), 2.
[18] J. Thévenot, H. Oliveira, O. Sandre, S. Lecommandoux, Chem. Soc. Rev. 42 (2013) 7099.
[19] P.I.P. Soares, J. Romão, R. Matos, J.C. Silva, J.P. Borges, Prog. Mater. Sci. 116 (2021) 100742.
[20] Y. Kim, H. Yuk, R.K. Zhao, S.A. Chester, X.H. Zhao, Nature 558 (2018) 274.
[21] B.Q.Y. Chan, Z.W.K. Low, S.J.W. Heng, S.Y. Chan, C. Owh, X.J. Loh, ACS Appl. Mater. Interfaces 8 (2016) 10070.
[22] X.H. Zhao, J. Kim, C.A. Cezar, N. Huebsch, K. Lee, K. Bouhadir, D.J. Mooney, Proc. Natl. Acad. Sci. U.S.A. 108 (2011) 67.
[23] D.A. Gilroy, C. Hobbs, V. Nicolosi, C.T. Buckley, F.J. O'Brien, C.J. Kearney, Mrs Commun. 7 (2017) 367.
[24] T. Gong, W. Li, H. Chen, L. Wang, S. Shao, S. Zhou, Acta Biomater. 8 (2012) 1248.
[25] G.Z. Lum, Z. Ye, X.G. Dong, H. Marvi, O. Erin, W.Q. Hu, M. Sitti, Proc. Natl. Acad. Sci. U.S.A. 113 (2016) E6007.
[26] W. Hu, G.Z. Lum, M. Mastrangeli, M. Sitti, Nature 554 (2018) 81.

[27] G. Cadafalch Gazquez, H. Chen, S.A. Veldhuis, A. Solmaz, C. Mota, B.A. Boukamp, C.A. van Blitterswijk, J.E. ten Elshof, L. Moroni, ACS Nano 10 (2016) 5789.
[28] Q. Fu, Y. Si, C. Duan, Z. Yan, L. Liu, J. Yu, B. Ding, Adv. Funct. Mater. 29 (2019) 1808234.
[29] H. Wang, X. Zhang, N. Wang, Y. Li, X. Feng, Y. Huang, C. Zhao, Z. Liu, M. Fang, G. Ou, H. Gao, X. Li, H. Wu, Sci. Adv. 3 (2017), e1603170.
[30] Y. Zhang, J. Li, M. Soleimani, F. Giacomini, H. Friedrich, R. Truckenmüller, P. Habibovic, Adv. Funct. Mater. 31 (2021) 2102911.
[31] L.C. Palmer, C.J. Newcomb, S.R. Kaltz, E.D. Spoerke, S.I. Stupp, Chem. Rev. 108 (2008) 4754.
[32] C. Shuai, W. Yang, P. Feng, S. Peng, H. Pan, Bioact. Mater. 6 (2021) 490.
[33] P. Feng, S. Peng, C. Shuai, C. Gao, W. Yang, S. Bin, A. Min, ACS Appl. Mater. Interfaces 12 (2020) 46743.
[34] C. Shuai, B. Peng, P. Feng, L. Yu, R. Lai, A. Min, J. Adv. Res. 35 (2022) 13.
[35] S.M. Dadfar, K. Roemhild, N.I. Drude, S. von Stillfried, R. Knuchel, F. Kiessling, T. Lammers, Adv. Drug Deliv. Rev. 138 (2019) 302.
[36] S.J. Dong, Y. Chen, L.D. Yu, K.L. Lin, X.D. Wang, Adv. Funct. Mater. 30 (2020), 1907071.
[37] C.T. Wu, W. Fan, Y.F. Zhu, M. Gelinsky, J. Chang, G. Cuniberti, V. Albrecht, T. Friis, Y. Xiao, Acta Biomater. 7 (2011) 3563.
[38] A. Farzin, M. Fathi, R. Emadi, Mater. Sci. Eng. C Mater. Biol. Appl. 70 (2017) 21.
[39] A. Jasemi, B.K. Moghadas, A. Khandan, S. Saber-Samandari, Ceram. Int. 48 (2022) 1314.
[40] M. Filippi, B. Dasen, J. Guerrero, F. Garello, G. Isu, G. Born, M. Ehrbar, I. Martin, A. Scherberich, Biomaterials 223 (2019), 119468.
[41] K.-Y. Qian, Y. Song, X. Yan, L. Dong, J. Xue, Y. Xu, B. Wang, B. Cao, Q. Hou, W. Peng, J. Hu, K. Jiang, S. Chen, H. Wang, Y. Lu, Biomaterials 259 (2020) 120299.
[42] J. Li, Z. Li, D. Chu, L. Jin, X. Zhang, J. Biomed. Nanotechnol. 15 (2019) 500.
[43] C.J. Shuai, Y. Cheng, W.J. Yang, P. Feng, Y.W. Yang, C.X. He, F.W. Qi, S.P. Peng, Compos. B Eng. 192 (2020), 107986.
[44] S. Hao, Y. Zhang, J. Meng, J. Liu, T. Wen, N. Gu, H. Xu, ACS Appl. Mater. Interfaces 10 (2018) 22913.
[45] M.M. Fernandes, D.M. Correia, C. Ribeiro, N. Castro, V. Correia, S. Lanceros-Mendez, ACS Appl. Mater. Interfaces 11 (2019) 45265.
[46] Q.W. Wang, B. Chen, F. Ma, S.K. Lin, M. Cao, Y. Li, N. Gu, Nano Res. 10 (2017) 626.
[47] H. Li, Y.J. Zhu, Y.Y. Jiang, Y.D. Yu, F. Chen, L.Y. Dong, J. Wu, Chemnanomat 3 (2017) 259.
[48] Y.G. Zhang, Y.J. Zhu, Z.C. Xiong, J. Wu, F. Chen, ACS Appl. Mater. Interfaces 10 (2018) 13019.
[49] C. Siangsanoh, S. Ummartyotin, K. Sathirakul, P. Rojanapanthu, W. Treesuppharat, J. Mol. Liq. 256 (2018) 90.
[50] Y. Deng, J. Chen, J. Huang, X. Yang, X. Zhang, S. Yuan, W. Liao, Cellulose 27 (2020) 3971.
[51] M. Sadat-Shojai, M.-T. Khorasani, E. Dinpanah-Khoshdargi, A. Jamshidi, Acta Biomater. 9 (2013) 7591.
[52] C. Li, J. Wang, Y. Wang, H. Gao, G. Wei, Y. Huang, H. Yu, Y. Gan, Y. Wang, L. Mei, H. Chen, H. Hu, Z. Zhang, Y. Jin, Acta Pharm. Sin. B 9 (2019) 1145.
[53] J. Li, S. Song, J. Meng, L. Tan, X. Liu, Y. Zheng, Z. Li, K.W.K. Yeung, Z. Cui, Y. Liang, S. Zhu, X. Zhang, S. Wu, J. Am. Chem. Soc. 143 (2021) 15427.
[54] G. Parekh, Y. Shi, J. Zheng, X. Zhang, S. Leporatti, Ther. Deliv. 9 (2018) 451.
[55] H. Peng, X. Zhang, P. Yang, J. Zhao, W. Zhang, N. Feng, W. Yang, J. Tang, Bioact. Mater. (2021), https://doi.org/10.1016/j.bioactmat.2021.12.018.
[56] H. Shi, S. Yang, S. Zeng, X. Liu, J. Zhang, J. Zhang, T. Wu, X. Ye, T. Yu, C. Zhou, J. Ye, Appl. Mater. Today 15 (2019) 100.
[57] Y.G. Zhang, Y.J. Zhu, F. Chen, B.Q. Lu, Colloids Surf. B Biointerfaces 159 (2017) 337.
[58] C. Shuai, Y. Cheng, W. Yang, P. Feng, Y. Yang, C. He, F. Qi, S. Peng, Compos. B Eng. 192 (2020) 107986.
[59] C.J. Shuai, W.J. Yang, C.X. He, S.P. Peng, C.D. Gao, Y.W. Yang, F.W. Qi, P. Feng, Mater. Des. 185 (2020), 108275.